Many-body coherence effects in conduction through a quantum dot in the fractional quantum Hall regime

Jari M. Kinaret, Yigal Meir,* Ned S. Wingreen,* Patrick A. Lee, and Xiao-Gang Wen
Department of Physics, Massachusetts Institute of Technology, Cambridge, Massachusetts 02139
(Received 13 April 1992)

We study a quantum dot in the fractional quantum Hall regime by solving the problem exactly for up to eight electrons at filling factors between 1 and $\frac{1}{3}$. Many-body coherence in the fractional regime strongly suppresses the resonant conductance through a weakly coupled dot below the integer regime values. In particular, using the edge-wave theory of excitations, we predict that, at low temperatures and small bias voltages, all conductance peaks are lowered by a factor of $1/N$ at $\nu=\frac{1}{3}$, and that at $\nu=\frac{2}{3}$ odd and even peaks are suppressed differently. We also show that strongly coupled excited states lead to an anomalous temperature dependence of the resonance peaks, whereas weakly coupled excited states can be identified from the line shapes in nonlinear measurements.

I. INTRODUCTION

Advances in microfabrication techniques have recently made it possible to fabricate electronic devices on the nanometer scale. The physics of electron interaction in these new devices has attracted a great deal of both experimental and theoretical interest. In particular, the capacitances of the devices are so small ($\approx 10^{-16}$ F) that any change in the number of electrons changes the total energy appreciably. This has opened interesting experimental possibilities relating to charging effects in small structures. For example, periodic resonances have been observed in the conductances of these devices as a function of gate voltage in the absence[1] or presence[2] of a magnetic field.

Recent studies have clearly demonstrated the importance of Coulomb interactions in small samples.[3,4] The interactions have two conceptually different effects in small electronic systems. First, they lead to the phenomena known as Coulomb blockade,[5] which is a manifestation of charge quantization due to the small capacitance of the system. The second effect of electron-electron interactions, which can be seen also in macroscopic samples, is to introduce nontrivial correlations in the many-electron wave function. This effect is responsible for the formation of fractional quantum Hall (FQH) states in macroscopic samples,[6] and it is interesting to see how the FQH states manifest themselves in small samples, where charge quantization effects are important. It is especially interesting because the small capacitance allows one to study experimentally the relation between a state of $(N-1)$ or N electrons in the dot, which could shed light on the non-Fermi-liquid behavior of the FQH system.

A good way to study that relation is through conductance measurements as a conductance process inevitably involves a change in the number of electrons in the system. Until our work[7] no theoretical predictions existed for conductance through quantum dots in the fractional regime, although the problem had been studied in the integer regime.[8,9] In this paper we solve the problem exactly for up to eight interacting electrons in a quantum dot in the FQH regime, and also make analytic predictions based on the edge-wave theory of excitations.

Our work focuses on the experimentally observable effects of many-electron correlations in a quantum dot in the FQH regime. In particular, we predict that at low temperatures and small bias voltages many-body coherence leads to a strong, filling factor-dependent suppression of the conductance between two electrodes coupled weakly to each other via the dot. At temperatures larger than the excitation gap, and at finite bias voltages, transport through excited states is allowed and the predictions are modified somewhat. The good agreement between our exact wave functions and those based on Laughlin states lead us to believe that these predictions are valid for larger dots as well. Many of the results for low temperatures and small bias voltages have been published in an earlier Rapid Communication.[7] In this paper, we discuss the validity of our approximations in more detail, report our results at finite temperatures and bias voltages, and extend the analytic discussion to filling factor $\nu=\frac{2}{3}$.

II. EXPERIMENTAL SETUP

The central feature of the experimental setup we have in mind is a quantum dot, which is usually fabricated by using either gate electrodes or etching to laterally confine electrons in a two-dimensional electron gas at a semiconductor heterointerface (Fig. 1). The radius of the electron charge distribution is typically 100–200 nm. The dot is coupled weakly to two external leads the chemical potentials of which are μ_L and μ_R. The weak links are established either electrostatically by means of narrow constrictions (in planar structures), or by separating the dot from leads by a larger band-gap material (in vertical structures). A bias voltage can be applied between the two leads so that $\mu_L > \mu_R$. A third electrode, the gate, is used in the planar geometry to control the number of electrons in the dot, which in a typical experimental arrangement is approximately 100. In the vertical

 ©1992 The American Physical Society

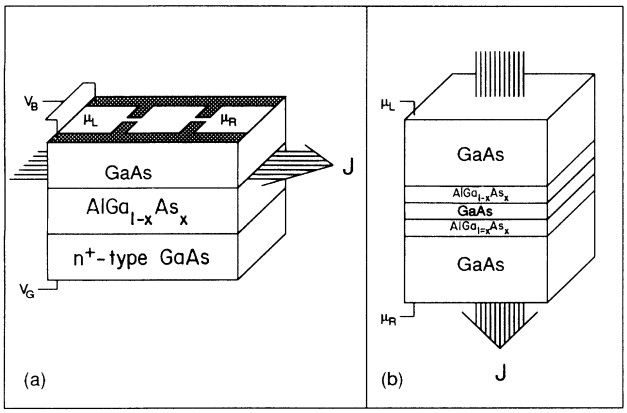

FIG. 1. (a) Planar experimental geometry (Refs. 2 and 11). Negative voltage $-V_T$ is applied to the top gate, which expels electrons in the two-dimensional electron gas and creates a laterally confined quantum dot. The dot is weakly coupled to the leads through electrostatic tunnel barriers, which are also formed using the top gate (i.e., the leads L or R are in the same plane as the dot). The back gate voltage V_G is used to control the number of electrons in the dot. The chemical potentials μ_L and μ_R are set by external reservoirs. (b) Vertical experimental geometry (Refs. 24 and 23). Electrons in the central GaAs layer are weakly coupled to the leads through the narrow $AlGa_{1-x}As_x$ barriers (i.e., the leads L or R are directly above and below the quantum dot). Lateral confinement is obtained through ion bombardment or chemical etching. No gate electrode has been built in.

geometry experiments no gate electrode has been used. In the experiments we are considering, a strong magnetic field is applied in a direction perpendicular to the heterointerface, and the current between the external leads is measured as a function of gate voltage and magnetic field. A current or conductance peak is observed when the chemical potential in the leads coincides with the energy required to add an electron to the dot.

So far the experiments have been performed in the regime where several Landau levels are occupied (the integer quantum Hall regime),[2] and the study of the movement and relative heights of the conductance peaks has provided detailed information of the electronic structure of the dot. We expect that similar experiments in the FQH regime, i.e., when only one Landau level is occupied, will be performed shortly.[10] The conductance experiments in the fractional regime that have been performed so far were conducted at a fairly strong coupling between the dot and the leads,[11] which is different from the limit we study.

III. MODEL

We consider an interacting two-dimensional electron gas, in a magnetic field, confined in the plane by a parabolic potential and described by the Hamiltonian

$$H=\frac{1}{2m}\sum_{i=1}^{N}[-i\hbar\nabla_i-e\,\mathbf{A}(\mathbf{r}_i)]^2+\tfrac{1}{2}m\omega_0^2\sum_{i=1}^{N}r_i^2+\sum_{i<j}v(|\mathbf{r}_i-\mathbf{r}_j|)\ . \tag{1}$$

The parabolic approximation for the confining potential has been shown to be remarkably accurate in the common experimental geometries employing the planar structure.[1,12] It is, of course, also very convenient mathematically, as we will point out later. In the planar geometry device that was used by McEuen *et al.* the curvature of the confining potential corresponds to $\hbar\omega_0=1.6$ meV,[2,3] which is approximately equal to the cyclotron energy at 1 T. Throughout this paper we limit our discussion to the regime of sufficiently high magnetic fields perpendicular to the plane such that only the lowest Landau level is occupied. This approximation is justified very well in extended fractional quantum Hall samples,[13] and we will argue that it remains justified for a parabolic dot in the fractional quantum Hall regime.

Since the Hamiltonian H is cylindrically symmetric (in symmetric gauge), it commutes with the (two-dimensional) angular momentum operator, and its eigenstates in the lowest Landau level can be written as

$$\psi_{M,\alpha}=\exp\left[-\tfrac{1}{4}\sum|z_i|^2\right]\times\prod_{i<j}(z_i-z_j)P_{M,\alpha}(z_1,\ldots,z_N)\ , \tag{2}$$

where $P_{M,\alpha}$ is an Mth-order symmetric polynomial of N variables and $z_j=x_j+iy_j$ gives the coordinate (x_j,y_j) of the jth electron. It is a special feature of the parabolic potential that the length scales of the magnetic field and the confining potential combine to just one length scale, the effective magnetic length $l_{\rm eff}(B)$, which is given by $l_{\rm eff}^{-2}(B)=m\omega_{\rm eff}/\hbar$, where $\omega_{\rm eff}=(4\omega_0^2+\omega_c^2)^{1/2}$ and ω_c is the cyclotron frequency. Due to this property of the Hamiltonian the magnetic field only appears in the length scale and does not affect the functional form of the states. The simplest many-particle state that obeys the exclusion principle and is fully in the lowest Landau level is obtained by setting $P_{M,\alpha}(z_1,\ldots,z_N)=1$. That state is a Slater determinant of the lowest angular momentum single-particle states, and has filling factor $\nu=1$ and total angular momentum $L=N(N-1)/2$. Other states of the form (2) have angular momenta in excess of this value. The quantum number M denotes the *excess* angular momentum of a state so that the total angular momentum is given by $L=\frac{1}{2}N(N-1)+M$, and α enumerates the different eigenstates with the same M.

In the absence of electron-electron interactions, states with the same excess angular momenta are degenerate. This degeneracy is broken by interactions, and the energy is given by

$$E_{N,M,\alpha}=\frac{\hbar\omega_{\rm eff}}{2}[N+L(1-\omega_c/\omega_{\rm eff})+\tfrac{1}{2}N(N-1)\xi_{N,M,\alpha}]\ , \tag{3}$$

where $\xi_{N,M,\alpha}$ is the expectation value of the electron-electron interaction $V(r)$ in the many-body eigenstate $\psi_{M,\alpha}$. The first term in the energy can be viewed as the kinetic energy of electrons in the lowest Landau level, the second term is the potential energy due to the confining potential, and the last term is the interaction energy. From this expression for the energy we can see that in-

cluding only the lowest Landau level is justified in the discussion of the lowest energy states of a noninteracting system if $l_{\max} < (\omega_c/\omega_0)^2$, or $N < (\omega_c/\omega_0)^2$, where $l_{\max}$ is the maximum single-particle angular momentum; for an interacting system it is justified more generally because the interaction energy decreases with increasing system size or increasing angular momentum.

IV. EXACT DIAGONALIZATION

We now proceed to find $\psi_{M,\alpha}$, the exact N-electron eigenstates. Since the interaction does not couple many-particle states with different angular momenta, we solve each angular momentum separately in three steps: (a) enumerate all possible N-particle basis states $|NM\beta\rangle$ with a given angular momentum, (b) calculate the interaction matrix $\langle NM\beta'|V|NM\beta\rangle$, (c) diagonalize the matrix.

To facilitate step (a) we use the fact that the center-of-mass coordinate separates in our problem, which is another consequence of the particular form for the confining potential. A state with center-of-mass angular momentum $L_{\text{c.m.}}$ can be written as $\psi_{L_{\text{c.m.}}} = z_{\text{c.m.}}^{L_{\text{c.m.}}} \cdot \psi_{L_{\text{c.m.}}=0}$, and has energy $E_{L_{\text{c.m.}}} = E_{L_{\text{c.m.}}=0} + L_{\text{c.m.}} \hbar\omega_{\text{eff}}(1-\omega_c/\omega_{\text{eff}})/2$, where $z_{\text{c.m.}}$ is the complex center-of-mass coordinate $z_{\text{c.m.}} = 1/N \sum z_i$. The center-of-mass motion can be probed by cyclotron resonance experiments,[14] and has been theoretically studied earlier.[15] In conductance measurements, on the other hand, the lowest energy states are most important, and it turns out that only states with $L_{\text{c.m.}} = 0$ contribute to conductance at low temperatures, as we will show later.

In the following we construct states which explicitly exclude the center-of-mass motion. We start from the primitive symmetry polynomials $\sigma_N^{(h)}$, which are given by sums of all h-term products of N variables, i.e., $\sigma_N^{(1)} = \sum z_i$, $\sigma_N^{(2)} = \sum_{i<j} z_i z_j$, $\sigma_N^{(3)} = \sum_{i<j<k} z_i z_j z_k$, etc. All symmetric polynomials of N variables can be written as sums of products of primitive symmetric polynomials.[16,17] To exclude the center-of-mass component we perform a change of variables and consider σ's of the variables $z_i - z_{\text{c.m.}}$. The products of these polynomials can be used as a basis of symmetric polynomials of order M without center-of-mass motion. The exclusion of center-of-mass degrees of freedom reduces the number of basis states significantly: for example, for $N=5$ electrons there are 13 states with excess angular momentum $M=7$, but only three of them contain no center-of-mass motion.

In the exact diagonalization of the Hamiltonian for small systems we take the interaction potential to be $V(r) = Q^2\hbar^2/2mr^2$, which allows us to evaluate the interaction matrix elements *analytically* [step (b)]. The coupling strength Q^2 is only a scale factor in the last term in (3) and has been set equal to 1 in the subsequent discussion. This choice is different from the actual interaction potential in the experimental systems, which is Coulombic r^{-1} at intermediate distances, varies more slowly at short distances due to the finite thickness of the electron gas, and at large distances turns over to a r^{-3} behavior due to image charges in the gate electrodes. However, it has been shown that the FQH effect is quite robust against variations in the interparticle potential,[18] and in particular the short-range differences are suppressed by the exclusion principle. Consequently, we expect the r^{-2} potential to give reliable qualitative results.

In order to interpret our results and make experimental predictions for larger dots we want to label the exact eigenstates in a way which can be extended to larger systems. Therefore, we first construct an average filling factor ν_{av}. The average filling factor is constructed by approximating the charge distribution of an exact many-electron eigenstate with a uniform charge distribution with a sharp edge. The density and radius of the uniform charge distribution are determined by requiring that the total charge and the expectation value $\langle r^2\rangle$ agree with the exact solution. Since for a uniform distribution $\langle r^2\rangle = R^2/2$, where R is the radius of the uniform distribution, we obtain $\nu_{\text{av}} = N\Phi_0/2\pi B\langle r^2\rangle = N^2/2(N+L)$. The second expression was obtained using $\langle r^2\rangle = 2l_B^2(N+L)/N$, which is valid for states in the lowest Landau level. For large N this agrees with the filling factor for Jastrow states $\nu_J = N(N-1)/2L$ (notice that L scales like N^2). We have solved the eigenstates of systems of 3–8 electrons up to excess angular momentum $M=18$ corresponding to average filling factors down to $\nu_{\text{av}}^{\min} = \frac{3}{16} \approx 0.19$ for $N=3$ and $\nu_{\text{av}}^{\min} = \frac{16}{27} \approx 0.59$ for $N=8$. The condition $l_{\max} < (\omega_c/\omega_0)^2$ is satisfied by all the exact solutions for $\omega_c > 4.5\omega_0$, so the approximation of including only the lowest Landau level is well justified for magnetic fields in the FQH regime.

While for large systems the filling factor is constant throughout the bulk, in small systems the edge is much more important and the average filling factor only serves

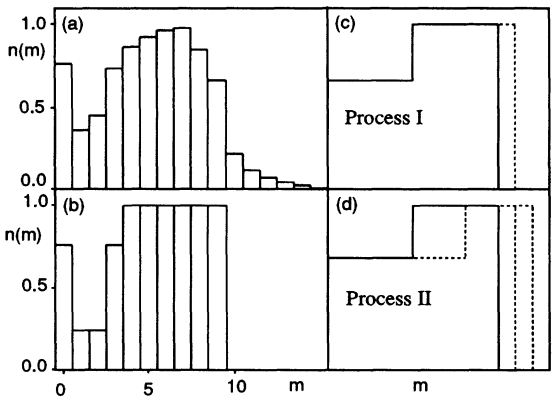

FIG. 2. (a) Occupations of single-particle states of definite angular momenta in the lowest eight-particle eigenstate with excess angular momentum $M=14$. (b) Occupations of single-particle states in the eight-electron particle-hole symmetric state with $P=2$ and $q=3$. The overlap between this state and the exact state shown in (a) is 0.75. (c) Schematic picture of the transition at $\nu = \frac{2}{3}$ from an $(N-1)$-particle state to an N-particle state through process I. Solid line: occupations near the edge of the system of $N-1$ particles; dashed line: occupations near the edge of the system of N particles. (d) Schematic picture of the transition through process II.

as a guide and does not specify the state uniquely. A more useful way to characterize a few-electron state is via $n(m)$, the occupation of single-particle states of definite angular momenta $m=0,1,2,\ldots$,[19,20]

$$n(m)=\langle c_m^\dagger c_m \rangle \ . \tag{4}$$

For the $\nu=1$ case, when the many-particle wave function is given by one Slater determinant, $n(m)$ is one for $m<N$ and zero otherwise. At filling factors $\nu<1$ the many-particle wave function is a linear combination of several Slater determinants, and $n(m)$ acquires a more complicated structure.

In Fig. 2(a) we display the occupations of single-particle states for the lowest energy eigenstate of eight electrons with excess angular momentum $M=14$. At particular filling factors, for large N, it has been suggested that the ground states are given by the particle-hole symmetric counterparts of Laughlin states[21]

$$\psi_{N,P,q}^{\nu=1-1/q}(z_1,\ldots,z_N) = \int \left[\prod_{h=1}^{P} d^2 z_{N+h} \right] \psi_{N+P}^{(\nu=1)}(z_1,\ldots,z_{N+P}) \times [\psi_P^{(\nu=1/q)}(z_{N+1},\ldots,z_{N+P})]^* \ . \tag{5}$$

Specifically, these N-electron wave functions are described by P holes in the $1/q$ Laughlin state in a background of $N+P$ electrons in the $\nu=1$ state. These Laughlin-type states have excess angular momenta

$$M=P\left[N-\frac{q-1}{2}(P-1)\right] ,$$

and have core filling factors $\nu=1-1/q$ over the central fraction of the dot, in the large-N limit. For example, the state with $N=8$, $P=2$, and $q=3$ has $M=14$. Different choices of P correspond to different edge structures and we cannot say *a priori* which of them is energetically favorable. The single-particle occupations in this state are shown in Fig. 2(b), and the resemblance to $n(m)$ of the exact lowest energy eigenstate suggests the identification of the latter as a $\nu=\frac{2}{3}$ particle-hole symmetric state. We find that for those M for which a particle-hole symmetric construction exists, the lowest eigenstate can be identified in this way. The overlap between the exact many-particle state and the corresponding particle-hole symmetric construction varies from 0.6 to 0.8 for those states that could be identified. These overlaps are large enough to allow us to label the exact states in the same fashion as the particle-hole symmetric ansatz states, i.e., in terms of holes occupying correlated FQH states with simple filling factors, although the Ansatz states should not be used to calculate quantities like the ground-state energy.

We want to point out that we have made no approximations and our solutions are the exact eigenstates of (1). In this respect our work is different from that of Johnson and MacDonald,[20] who considered quantum dots with more electrons than we do in the present finite-size calculation. However, they used a severe truncation method to restrict the single-particle Hilbert space, and their solutions are not exact. It turns out that although the truncation does not appreciably change the energies of the lowest-lying states, it does significantly affect the conductance properties of the system, at least for the r^{-2} interaction.

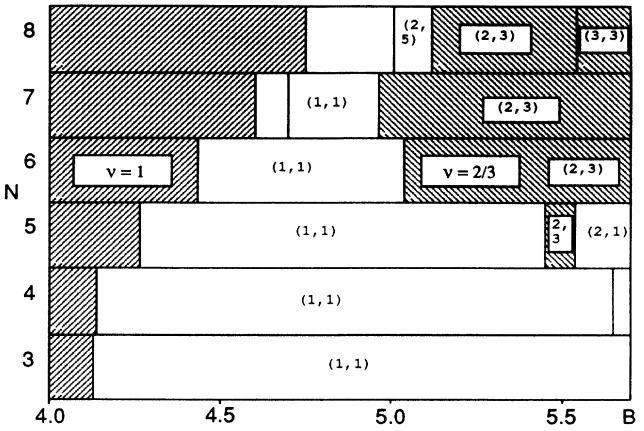

FIG. 3. Ground states of N-electron systems as a function of B in units of $m\omega_0/e$. The shaded regions correspond to $\nu=1$ and $\nu=\frac{2}{3}$. The notation (P,q) denotes a state which is well described by P holes in the $1/q$ state in the background of electrons in the $\nu=1$ state.

In Fig. 3 we show the ground states of systems with 3–8 electrons as a function of the magnetic field. All but two of them can be identified using particle-hole symmetry. [For compactness, the notation (P,q) denotes a state with P holes in the $1/q$ state.] The stability of the $\nu=\frac{2}{3}$ states (shaded in Fig. 3) increases with the number of particles as expected, and we see the appearance of a $\nu=\frac{4}{5}$ state for $N=8$. The $\nu=\frac{1}{3}$ states that we refer to later occur at stronger magnetic fields and do not appear in Fig. 3.

V. CONDUCTANCE IN LINEAR RESPONSE

A. Conductance through a weakly coupled dot

The conductance peaks arise because electrons can enter and leave the dot through the weak links to the leads. Throughout this paper we limit the discussion to the weak-coupling case, when the elastic broadening of states in the dot is much less than the excitation gap ($\Gamma_{el}\ll\Delta$). We describe the coupling between the dot and the leads with the tunneling Hamiltonian

$$H_T=\sum_{k,m}(t_{km}^L c_m^\dagger c_k^L + t_{km}^R c_m^\dagger c_k^R)+\text{H.c.} \ , \tag{6}$$

where $c_m^\dagger$ creates an electron in a single-particle state with angular momentum m in the dot and c_k^L or c_k^R annihilates an electron in a free single-particle state k in the left or the right lead, respectively. In discussing the conductance it is useful to introduce the elastic coupling matrix $\tilde{\gamma}^{\text{eff}}$, which is defined by

$$\tilde{\gamma}^{\text{eff}}=\frac{\tilde{\gamma}^L\tilde{\gamma}^R}{\tilde{\gamma}^L+\tilde{\gamma}^R} \ , \tag{7}$$

where

$$\gamma^L_{mn}=2\pi\sum_k t^L_{km}(t^L_{kn})^*\delta(\varepsilon^L_k-\mu) \tag{8}$$

with γ^R_{mn} defined analogously. Here ε^L_k is the energy of a single-particle state in the left lead. Provided that the couplings to the left and right leads are proportional, $\tilde{\gamma}^L=\lambda\tilde{\gamma}^R$, the linear-response conductance through the dot is given by[22,8]

$$\sigma(\mu,B)=\frac{e^2}{h}2\pi\int_{-\infty}^{\infty}d\varepsilon[-f'_{\rm FD}(\varepsilon)]\times\left[-\frac{1}{\pi}{\rm Im}[{\rm Tr}\{\tilde{\gamma}^{\rm eff}\tilde{G}_{\rm ret}\}]\right]. \tag{9}$$

The retarded Green's function $\tilde{G}_{\rm ret}$ is a matrix with elements given by

$$G_{nm}=-i\Theta(t)\langle\{c_n(t),c^\dagger_m(0)\}\rangle\ ,$$

where the expectation value is evaluated for the interacting system including the leads.

The linear-response conductance through a quantum dot changes in an interesting fashion as a function of temperature. We can identify three different temperature regimes. At very low temperatures the elastic broadening of conductance peaks is more important than the thermal broadening, $k_BT\ll\Gamma_{\rm el}$, and a true resonant-tunneling behavior is expected. At intermediate temperatures the thermal broadening is larger than the elastic broadening, but less than the excitation gap in the dot, $\Gamma_{\rm el}\ll k_BT\ll\Delta$. In this temperature range the transport is still governed by ground-state properties of the dot, but the behavior is different from the low-temperature regime, as we will demonstrate later. Finally, if the temperature is larger than the excitation gap, $\Delta\ll k_BT$, transport through excited states is allowed. The low- and intermediate-temperature regimes are quite similar, so we will discuss them first, and mostly concentrate on the intermediate-temperature regime.

B. Conductance at intermediate temperatures

When the elastic broadening is less than the temperature and the excitation gap, $\Gamma_{\rm el}\ll k_BT$ and $\Gamma_{\rm el}\ll\Delta$, the conductance formula can be simplified to[9]

$$\sigma(\mu,B)=\frac{e^2}{h}2\pi\sum_N\sum_{M,M'}\sum_{\alpha,\alpha'}\Gamma^{\rm eff}_{M\alpha,M'\alpha'}[-f'_{\rm FD}(E_{N,M,\alpha}-E_{N-1,M',\alpha'}-\mu)][P_{\rm eq}(N,M,\alpha)+P_{\rm eq}(N-1,M',\alpha)]\ , \tag{10}$$

where the effective couplings between many-particle states are given by

$$\Gamma^{\rm eff}_{M\alpha,M'\alpha'}=\gamma^{\rm eff}_{\Delta L,\Delta L}|\langle N,M,\alpha|c^\dagger_{\Delta L}|N-1,M',\alpha'\rangle|^2 \tag{11}$$

and $\gamma^{\rm eff}_{mm}$ is a diagonal element of the elastic coupling matrix (7). In Eq. (11) ΔL is the difference between the angular momenta of states $|N,M,\alpha\rangle$ and $|N-1,M',\alpha'\rangle$. In the subsequent discussion we will often use the quantities Γ^L and Γ^R, which are related to γ^L and γ^R in the same way as $\Gamma^{\rm eff}$ is related to $\gamma^{\rm eff}$. The total elastic broadening is $\Gamma_{\rm el}=\Gamma^L+\Gamma^R$. Here we have made the assumption that the inelastic scattering in the dot is weak, $\Gamma_{\rm inel}\ll k_BT$ and $\Gamma_{\rm inel}\ll\Delta$.

The expression (10) for the conductance is a product of three terms. The first term determines the relative heights of conductance peaks and the second term determines the positions and shapes of the peaks. The last term, which is the sum of grand canonical equilibrium probabilities of the dot being in one of the states that participate in a particular transition, reduces to one near the center of a conductance peak at low temperatures. The effective many-particle coupling $\Gamma^{\rm eff}$ consists of a single-particle contribution $\gamma^{\rm eff}$ and a many-particle part, which measures the overlap between the state of $N-1$ electrons, plus one additional electron with the appropriate angular momentum $\Delta L=N-1+(M-M')$, and the state of N electrons. In the integer regime this overlap is unity but in the fractional regime it can be significantly less than one. The single-particle coupling is a smooth function of ΔL, and in the following we shall set it equal to a constant. This choice corresponds more closely to a vertical geometry,[23,24] where all angular momentum states are coupled equally strongly to the leads. In the more common planar geometry[2,11] states with larger angular momenta are closer to the leads and couple more strongly, and γ_{mm} is a monotonically increasing function of m. The effects of a varying single-particle coupling have been studied in the integer quantum Hall regime and can easily be accounted for also in the fractional regime. However, for simplicity we will now concentrate on the many-body effects which affect the overlap matrix element.

In the low-temperature regime, $k_BT\ll\Gamma^L,\Gamma^R\ll\Delta$, a true resonant behavior is expected. In that case the height of a conductance peak is proportional to $\Gamma^L\Gamma^R/[(\Gamma^L+\Gamma^R)^2/4+(\Delta E)^2]$, which reduces to one at resonance for $\Gamma^L=\Gamma^R$. The linewidth of a resonance peak at low temperatures is given by $(\Gamma^L+\Gamma^R)$, and consequently we expect many-body coherence effects to reduce the linewidth below the integer regime values. In the remainder of this paper we choose to concentrate on the intermediate temperature case $k_BT\gg\Gamma^L,\Gamma^R$.

1. Finite-size studies

Since the finite-size study is done using first-quantized notation and the expression (10) for the conductance is in the second-quantized form, we must establish a connection between the two formalisms. Let us denote the first-quantized wave function for N particles by $\Psi_N(z_1,\ldots,z_N)=\mathcal{A}_N[\phi(z_1,\ldots,z_N)]$, where $\mathcal{A}_N$ is the antisymmetrizating operator for N variables. By doing the explicit calculation it is easy to see that the state $c^\dagger_m\psi_N$ is

$$c_m^\dagger \psi_N(z_1,\ldots,z_N)=(N+1)^{-1/2}\mathcal{A}_{N+1}[(2\pi 2^m m!)^{-1/2} z_{N+1}^m e^{-(1/4)|z_{N+1}|^2}\phi(z_1,\ldots,z_N)]\ , \tag{12}$$

where the prefactor $(N+1)^{-1/2}$ arises for permutational reasons.

We first evaluated the overlap matrix element between $\nu=\frac{1}{3}$ Laughlin state with $(N-1)$ and N particles and found that it decreases as $(N-\frac{1}{2})^{-1/2}$ (Fig. 4). We also evaluated the overlap matrix element between the exact lowest-energy eigenstates of H at filling factor $\frac{1}{3}$. The results agree with those obtained for the Laughlin state to within 3.5% and 2.5% for $N=4$ and 5, respectively. This suggests that the Laughlin state is a good approximation of the exact ground state at filling factor $\nu=\frac{1}{3}$.

Our numerical results for the overlap matrix element in the $\nu=\frac{2}{3}$ case are shown in Table I. The notation is the same as in Fig. 3, i.e., $(P,q=3)$ denotes that exact eigenstate of H (not necessarily a ground state), which can be identified as a particle-hole symmetric state with P holes in state $\frac{1}{3}$. The empty entries are due to the fact that states with three holes can only be identified for $N=7$ and 8. We see that columns (a) and (b) are close to unity, whereas columns (c) and (d) give smaller overlaps. Column (a) extrapolates to a constant in striking contrast to the $(N-\frac{1}{2})^{-1/2}$ behavior in the $\nu=\frac{1}{3}$ case. Energetically favorable transitions are either of the form (I) $|N-1,P,q=3\rangle \rightarrow |N,P,3\rangle$ [columns (a) and (b)], where the electron is added to the outermost edge as shown in Fig. 2(c), or of the form (II) $|N-1,P,3\rangle \rightarrow |N,P+1,3\rangle$ [column (c)], shown in Fig. 2(d). Column (d) describes an energetically very costly transition in which the $\nu=\frac{2}{3}$ core shrinks when an electron is added to the system. Process II can be thought of as process I plus a particle-hole excitation whereby an electron is transferred from the inside to the outside edge, thereby expanding the $\nu=\frac{2}{3}$ region.

In order to preserve the $n\,(m)$ structure of the edge region and keep the filling factor constant, processes I and II must alternate as electrons are added to the dot. Thus in a measurement of conductance versus gate voltage we expect the heights of successive peaks to be different because of the different overlap factors. This doubling of the periodicity with N is expected on the general ground that for $\nu=\frac{2}{3}$ two added electrons are required to change the flux by an integer amount, i.e., it is impossible to keep the correlations unchanged when only one electron is added. The I, II ordering of the peaks may switch as a function of N or the magnetic field as the structure of the edge region evolves, but its detailed description is beyond the scope of the present small-N study.

As the magnetic field is varied at core filling factor $\nu=\frac{2}{3}$, the height and position of a given conductance peak vary smoothly except at some magnetic-field values, when the height changes abruptly. These sudden changes are due to a change of the ground state of either the N- or $(N-1)$-particle system (Fig. 5), and the height of a given peak as a function of the magnetic field should exhibit an alternating pattern similar to the alternation of peak heights versus gate voltage. In our numerical study we see one example of this behavior: the peak that corresponds to $7\leftrightarrow 8$ electrons in the dot is due to process I for $B<5.53$ and to process II for $B>5.53$ (Fig. 3), so that the height of the peak is lower by a factor $(0.248/0.654)^2=0.14$ (Table I) for $B>5.53$. The dependence of the single-particle couplings γ^L_{mm} and γ^R_{mm} on angular momentum and geometry may modify this prediction.

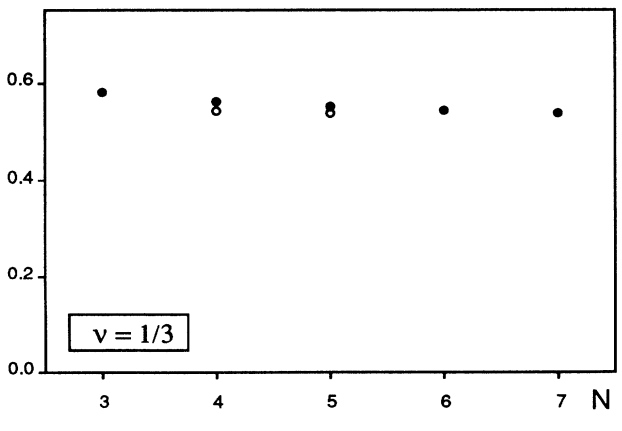

FIG. 4. Overlap matrix elements between $N-1$ and N-particle ground states for $\nu=\frac{1}{3}$, multiplied by $(N-\frac{1}{2})^{1/2}$. Filled dots are for Laughlin states and open dots are for the exact eigenstates. The convergence to a constant suggests an $N^{-1/2}$ behavior for the overlap matrix elements.

2. *Analytic results*

There is a simple way to understand the above results for $\nu=\frac{1}{3}$ in the thermodynamic limit. We consider a confining potential that is steep enough so that the width of the compressible region at the edge of the sample is no more than a couple of magnetic lengths. This assumption is valid for the parabolic confining potential at the magnetic fields we studied. At the opposite limit of a smooth confining potential,[25] the simple edge structure is lost and the discussion needs to be modified.

First we notice that the low-energy excitations of a FQH system occur at the edge, where the excitation gap

TABLE I. Overlap matrix elements between $(N-1)$- and N-electron systems for $\nu=\frac{2}{3}$: (a) $\langle(2,3)|c^\dagger|(2,3)\rangle$; (b) $\langle(3,3)|c^\dagger|(3,3)\rangle$; (c) $\langle(3,3)|c^\dagger|(2,3)\rangle$; (d) $\langle(2,3)|c^\dagger|(3,3)\rangle$. The notation (P,q) denotes a state with P holes in the $1/q$ Laughlin state in the background of $N+P$ electrons in the $\nu=1$ state. Columns (a) and (b) correspond to process I in Fig. 2(c), while column (c) corresponds to process II in Fig. 2(d).

N	(a)	(b)	(c)	(d)
6	0.626			
7	0.636		0.344	
8	0.654	0.568	0.248	0.106

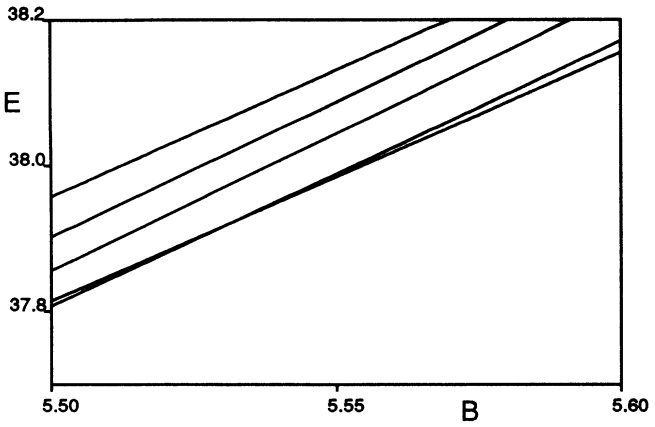

FIG. 5. Energies of the lowest states of a system of eight electrons as a function of the magnetic field. Energies are given in units of $\hbar\omega_0$ and the magnetic field is in units of $m\omega_0/e$. The lowest three states at $B=5.5$ can be identified as $|N=8,P=2,q=3\rangle$, $|8,3,3\rangle$, and $|8,2,5\rangle$; the higher states cannot be identified using particle-hole symmetry.

vanishes at the thermodynamic limit. The edge excitations of the $\nu=1/q$ state all move with the same velocity v. Thus for large x and t we may assume that the electron propagator is a function of $(x-vt)$ and has the form

$$G(x,t)=\langle \mathcal{T}_t[\psi(x,t)\psi^\dagger(0)]\rangle$$
$$=\exp(ik_Fx-iE_Ft)a^{\zeta-1}/(x-vt)^\zeta,$$

where a is a cutoff length scale ($a\approx l_B$), and x is the distance along the edge. It has been shown earlier by Wen[26] that the exponent ζ is equal to the inverse filling factor, $\zeta=q$. We now present a simple argument showing that this indeed is the case, and in addition we show that there is a direct connection between the exponent ζ and the scaling of conductance peaks.

For a Fermi liquid the exponent ζ in the electron propagator is equal to one. However, the strong correlations in a FQH system may change this behavior. We know that the ground-state total angular momentum of an N-electron system at filling factor $\nu=1/q$ is given by $L(N)=\frac{1}{2}qN(N-1)$. Therefore, adding an electron to the system increases the angular momentum by qN. This result suggests that, because of strong correlation, every electron occupies, on average, q single-particle states (in some sense electrons satisfy a "super Pauli principle"). In the following we will use this strong correlation effect to determine the exponent ζ.

For a quantum dot, which is large enough so that the electron propagator on the edge is given by the asymptotic form, we must require that $G(x,t)$ obeys periodic boundary conditions. Consequently, the propagator can be written as

$$G(R\theta,t)=\exp(im_F\theta-iE_Ft)a^{\zeta-1}R^{-\zeta}(1-e^{i(\theta-\bar{v}t)})^{-\zeta},$$

where R is the radius of the charge distribution and $\bar{v}=v/R$. For $t>0$ we may expand $G(R\theta,t)$ as

$$G(R\theta,t>0)=a^{\zeta-1}R^{-\zeta}e^{i(m_F\theta-E_Ft)}\times\left[\sum_{k=0}^{\infty}e^{ik(\theta-\bar{v}t)}\right]^\zeta. \quad (13)$$

For $t<0$ we must use a different expansion for the causal Green's function

$$G(R\theta,t<0)=(-1)^\zeta a^{\zeta-1}R^{-\zeta}e^{i[(m_F-\zeta)\theta-(E_F-\zeta\bar{v})t]}\times\left[\sum_{k=0}^{\infty}e^{-ik(\theta-\bar{v}t)}\right]^\zeta. \quad (14)$$

Another expression for G can be obtained from its definition as a nonequal time-correlation function. To do this, we first need to identify the ground state. Now we can evaluate the Green's function for $t>0$ by means of the spectral decomposition

$$G(R\theta,t>0)=\sum_m\sum_\alpha\langle N|\psi(0)|N+1,m,\alpha\rangle\times\langle N+1,m,\alpha|\psi^\dagger(0)|N\rangle\times e^{i[m+L(N+1)-L(N)]\theta}\times e^{-i[E_{m,\alpha}(N+1)-E_0(N)]t}, \quad (15)$$

where $|N+1,m,\alpha\rangle$ is an $(N+1)$-electron state with angular momentum $L(N+1)+m$ and energy $E_{m,\alpha}(N+1)$, and $E_0(N)$ is the ground-state energy. The $m=0$ term contains information about the $(N+1)$-particle ground state, and by comparison with the $k=0$ term of Eq. (13) we can read off both $m_F=L(N+1)-L(N)=qN$ and the overlap matrix element between ground states $|\langle N|\psi(0)|N+1\rangle|^2=a^{\zeta-1}R^{-\zeta}$. Fourier transforming to the angular momentum space yields a factor of $R^{1/2}$, and we get $|\langle N|c_{qN}|N+1\rangle|=(a/R)^{(\zeta-1)/2}\sim N^{-(\zeta-1)/4}$.

To determine the value of ζ we use the spectral expansion for $t<0$ to obtain

$$G(R\theta,t<0)=-\sum_m\sum_\alpha\langle N|\psi^\dagger(0)|N-1,m,\alpha\rangle\times\langle N-1,m,\alpha|\psi(0)|N\rangle\times e^{i[L(N)-L(N-1)-m]\theta}\times e^{-i[E_0(N)-E_{m,\alpha}(N-1)]t}. \quad (16)$$

Comparing the lowest energy term of this expansion with (14) we find $L(N)-L(N-1)=m_F-\zeta$ and obtain $\zeta=q$, which has to be an odd integer. Furthermore, from the time dependence we get $E_0(N)-E_0(N-1)=E_0(N+1)-E_0(N)-\zeta\bar{v}$, which shows that for a finite system there is a gap for edge excitations, which scales as $v/R\sim N^{-1/2}$.

Thus, we have shown that the edge-wave theory of excitations for FQH effect predicts that heights of conductance peaks at filling factor $\nu=1/q$ decrease as $N^{-(q-1)/2}$ as the number of electrons in the dot is increased. In particular, for the $\nu=\frac{1}{3}$ case we see that the absolute value of the matrix element decreases as $N^{-1/2}$, which is in agreement with the numerical results for small systems.

At more complicated filling factors there are several

branches of edge excitations, which move with different velocities. In particular, at $\nu=\frac{2}{3}$ there is a holelike branch on the inner edge and an electronlike branch on the outer edge. In this case we cannot follow the same method as for $\nu=\frac{1}{3}$ but we have to treat the problem more carefully. The low-energy edge excitations in the $\nu=\frac{2}{3}$ case are described by the effective Hamiltonian[27]

$$H_{\text{eff}}=2\pi v_1 q_1 \sum_{k>0}\rho_{1k}\rho_{-1k}+2\pi v_2 q_2 \sum_{k>0}\rho_{-2k}\rho_{2k} +2\pi\sqrt{|q_1 q_2|}\sum_{k>0} w_k(\rho_{1k}\rho_{-2k}+\rho_{2k}\rho_{-1k}) , \quad (17)$$

where ρ_1 and ρ_2 denote charge fluctuations at the inner and outer edge, respectively, and q_1 and q_2 are the *inverse* charges of the two excitation branches, i.e., $q_1=1$ and $q_2=-3$ (for $\nu=\frac{2}{3}$). The two edge waves move to opposite directions and consequently v_1 and v_2 have different signs: $v_1>0$ and $v_2<0$. The commutation relations for ρ_1 and ρ_2 can be derived by using the classical equation of motion $(\partial_t-v\partial_x)\rho=0$ to identify the canonical coordinates and momenta. We find that the quantum-mechanical operators ρ_1 and ρ_2 obey the algebra

$$[\rho_{1k},\rho_{1k'}]=\frac{k'}{2\pi q_1}\delta_{k+k'} , \qquad [\rho_{2k},\rho_{2k'}]=\frac{k'}{2\pi q_2}\delta_{k+k'} . \quad (18)$$

The Hamiltonian H_{eff} with commutation relations (18) describes a chiral Luttinger liquid with two branches, and it can be solved using the same methods as the standard Luttinger model.[28,29] The effective Hamiltonian is diagonalized by the transformation $e^{iS}H_{\text{eff}}e^{-iS}$, where

$$S=2\pi i\sqrt{|q_1 q_2|}\sum_{k>0}k^{-1}\theta_k(\rho_{1k}\rho_{-2k}-\rho_{2k}\rho_{-1k}) ,$$

and the angle θ_k is given by $\tanh(2\theta_k)=+2w_k/(v_1-v_2)$. To describe the propagation of electrons along the edge we must first write the electron creation and annihilation operators in terms of ρ_1 and ρ_2. An operator $\Psi^\dagger$ creates a particle with charge one on the edge if it satisfies the commutation relations

$$[\rho_1(x),\Psi^\dagger(y)]=n_1\Psi^\dagger(x)\delta(x-y) , \qquad [\rho_2(x),\Psi^\dagger(y)]=n_2\Psi^\dagger(x)\delta(x-y) , \quad (19)$$

where $n_1+n_2=1$. At filling factor $\nu=\frac{2}{3}$ both n_1 and n_2 are integers since the particle-hole excitations transfer an integer amount of charge between the inner and outer edges. For a general FQH state the edge structure may be more complicated allowing for a fractional charge transfer, thus, in general n_1 and n_2 may assume fractional values. Different choices of n_1 and n_2 correspond to different ways of adding charge to the system; in particular, process I corresponds to $n_1=1$, $n_2=0$, and process II corresponds to $n_1=2, n_2=-1$. Following Mattis and Lieb we find that the commutation relations (19) are satisfied by the operator

$$\Psi^\dagger(x)=\exp\left[-2\pi n_1 q_1\sum_{k>0}k^{-1}(e^{-ikx}\rho_{1k}-e^{ikx}\rho_{-1k})\right]\exp\left[-2\pi q_2 n_2\sum_{k>0}k^{-1}(e^{-ikx}\rho_{2k}-e^{ikx}\rho_{-2k})\right] , \quad (20)$$

which represents a particular way (characterized by n_1 and n_2) of increasing the charge of the system by one unit. Additionally, we must require that the operator Ψ is fermionic, i.e., $\Psi^\dagger(x)\Psi^\dagger(y)=-\Psi^\dagger(y)\Psi^\dagger(x)$. This condition is satisfied, provided that n_1 and n_2 are chosen so that $n_1^2 q_1+n_2^2 q_2$ is an odd integer.

Using the diagonalizing transformation an expression for the propagator $\langle\mathcal{T}[\Psi^\dagger(x,t)\Psi(0)]\rangle$ can be found in the same way as it is derived for the standard Luttinger model, and we obtain

$$G_{n_1 n_2}(x,t)\sim\exp\left[2\pi\sum_{k>0}k^{-1}[n_1\sqrt{|q_1|}\cosh(\theta_k)+n_2\sqrt{|q_2|}\sinh(\theta_k)]^2 e^{ik(x-\tilde{v}_{1k}t)}\right] \times\exp\left[2\pi\sum_{k>0}k^{-1}[n_1\sqrt{|q_1|}\sinh(\theta_k)+n_2\sqrt{|q_2|}\cosh(\theta_k)]^2 e^{-ik(x-\tilde{v}_{2k}t)}\right] ,$$

where $\tilde{v}_{1k}$ and $\tilde{v}_{2k}$ are the renormalized velocities

$$\tilde{v}_{1k}=\cosh^2(\theta_k)v_1-\sinh^2(\theta_k)v_2+\cosh(2\theta_k)w_k , \qquad \tilde{v}_{2k}=-\sinh^2(\theta_k)v_1+\cosh^2(\theta_k)v_2-\cosh(2\theta_k)w_k . \quad (21)$$

For a general interaction w_k these expressions are quite complicated, but if the interaction is short range, $w_k=w$, we obtain a particularly simple result

$$G_{n_1 n_2}(x,t)\sim(x-\tilde{v}_1 t)^{-[n_1\sqrt{|q_1|}\cosh(\theta)+n_2\sqrt{|q_2|}\sinh(\theta)]^2} \times(x-\tilde{v}_2 t)^{-[n_1\sqrt{|q_1|}\sinh(\theta)+n_2\sqrt{|q_2|}\cosh(\theta)]^2} . \quad (22)$$

The relation between the divergence of the propagator and the scaling of the overlap matrix element is the same

for complicated and simple filling factors, as can be seen by expanding the Green's function in a fashion similar to (13) and (15). Consequently, we expect that at $\nu=\frac{2}{3}$ process I gives rise to conductance peaks which decay as $N^{-\sinh^2(\theta)}$, and process II to peaks which decay as $N^{-[3-2\sqrt{3}\sinh(2\theta)+7\sinh^2(\theta)]}$. Our numerical results indicate that the heights of peaks due to process I remain constant independent of N, suggesting a very small θ [Table I, columns (a) and (b)]. This implies that the other peaks should decay as N^{-3}; however, we do not have enough numerical data to confirm this behavior.

It is interesting to note that at first glance this effect resembles the orthogonality catastrophe studied in connection with x-ray absorption in metals (see, e.g., Ref. 30). However, in x-ray absorption the orthogonality catastrophe arises because the single-particle states, which make up the Slater determinant, are different. In this case the single-particle states remain unchanged, but the linear combinations of Slater determinants that constitute the ground states are different. In x-ray absorption the relevant matrix element decreases as $N^{-\alpha/2}$, where α is between 0.05 and 0.1; in the case of the FQH dot the decay is considerably faster although still algebraic.

C. Conductance at higher temperatures

The results of the previous section are valid at low temperatures ($\Delta \gg kT \gg \Gamma^L, \Gamma^R$), when only transitions between the ground states contribute to the conductance. At higher temperatures several channels are active and carry current. (By a channel we mean the pair of quantum states $\{|N,\alpha\rangle, |N-1,\alpha'\rangle\}$ which allows an electron to be transmitted through the dot.) The threshold temperature above which thermal excitations are important depends on the size of the system and the magnetic field. The gap for edge excitations scales as $k \sim R^{-1}$, so the relevant temperature scale decreases as $N^{-1/2}$.

We will concentrate on the $\nu=\frac{2}{3}$ regime for 6–8 electrons in the dot and set for definiteness $\hbar\omega_0=1.6$ meV to fix the energy and temperature scales. In Figs. 6(a) and 6(b) we display calculated conductance versus gate-voltage curves at two magnetic fields and four temperatures ranging from 40 to 300 mK. The first peak corresponds to the number of electrons in the dot changing from 6 to 7, and the second peak corresponds to the addition of the eight electron. In Fig. 6(a) the magnetic field is 5.1 T ($\omega_c=5.5\omega_0$), and both ground-state transitions

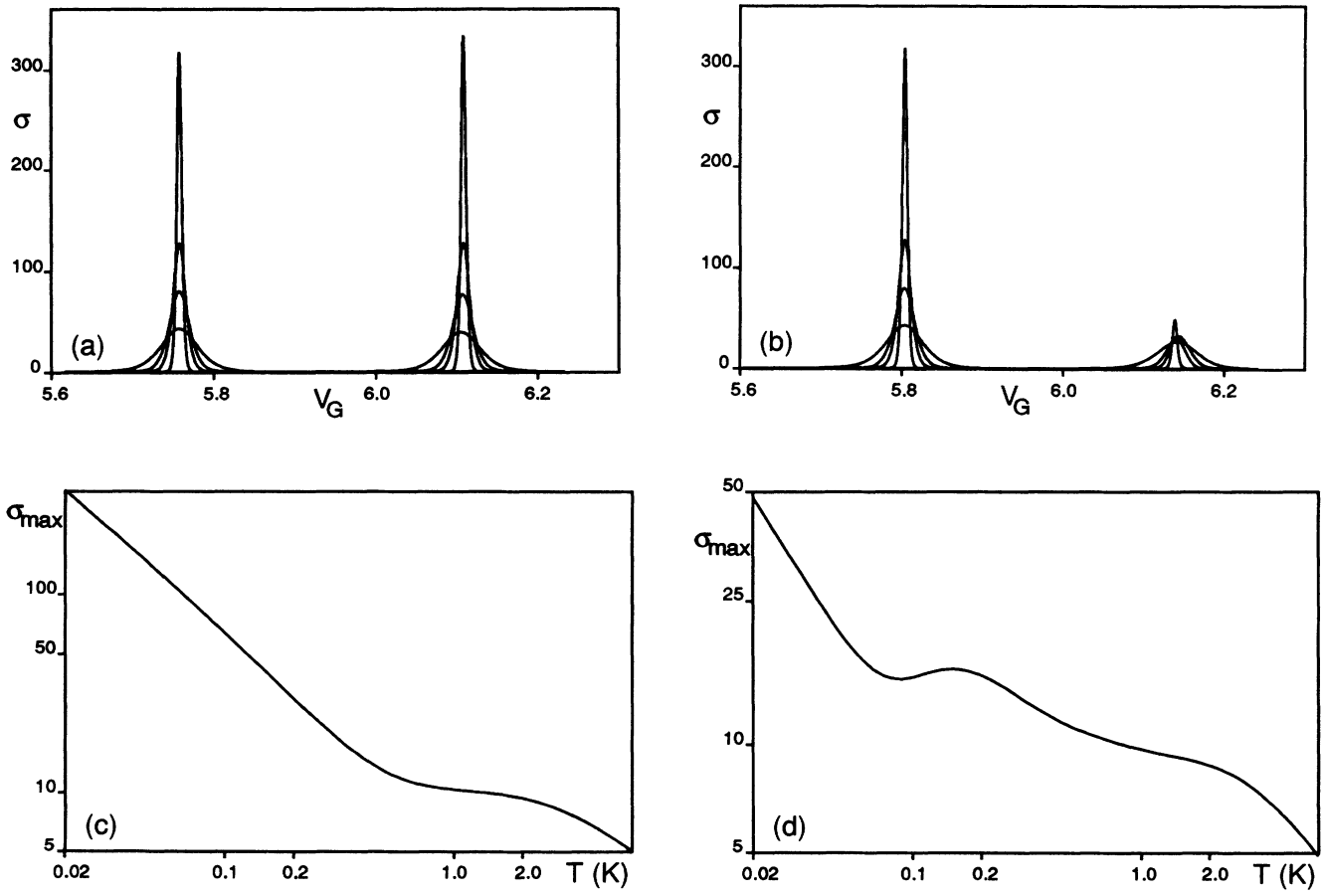

FIG. 6. Conductance as a function of the gate voltage at temperature $T=40$, 100, 150, and 300 mK ($\hbar\omega_0=1.6$ meV): (a) $B=5.1$ T, (b) $B=5.2$ T. The first peak corresponds to $N=6\leftrightarrow 7$ and the second peak to $N=7\leftrightarrow 8$. Maximum conductance for the peak $N=7\leftrightarrow 8$ as a function of temperature: (c) $B=5.1$ T, (d) $B=5.2$ T. Conductance is expressed in units of $(e^2/h)(\gamma/\hbar\omega_0)$.

$N=6\leftrightarrow 7$ and $N=7\leftrightarrow 8$ take place through process I. In Fig. 6(b) the magnetic field is 5.2 T ($\omega_c=5.6\omega_0$), so that the ground-state transition $N=7\leftrightarrow 8$ now occurs through process II, and the low-temperature conductance is consequently lower.

The dependence of the peak heights on temperature is shown in Figs. 6(c) and 6(d) for the $N=7\leftrightarrow 8$ peak at the two magnetic fields. At low temperatures the heights of both peaks decrease as $1/T$, as is expected if only one process contributes to the current. At $B=5.1$ T the excited channel starts to contribute to the current at temperatures of the order of $T_g=(E_{8,3,3}-E_{8,2,3})/k_B=130$ mK (Fig. 7), but due to the weak coupling of the excited channel the peak height continues to decrease as $1/T$ even at much higher temperatures. At $B=5.2$ T the gap for the excited channel is $T_g=(E_{8,2,3}-E_{8,3,3})/k_B=300$ mK, but since the excited channel is approximately seven times more efficient in carrying current than the channel involving the ground states, significant deviations from the $1/T$ behavior are seen already at temperatures $T_c=T_g/\log 13=120$ mK. The strongly coupled excited state also causes the center of the peak to shift to higher gate voltages as the temperature increases. Thus, an anomalous temperature dependence of a conductance peak indicates the existence of a well-coupled excited state. However, since the relative couplings of different channels are not known, it is difficult to construct an energy spectrum from finite-temperature measurements alone.

Anomalous temperature dependence of peak heights has been observed in the integer quantum Hall regime in the planar geometry.[2] In that case the couplings of channels are different because states in higher Landau levels are further away from the leads and their single-particle couplings γ_{mm} are consequently lower. Contrary to the integer case, in the fractional case we expect anomalous temperature dependence to be observable also in the vertical geometry, when all single-particle couplings are equal.

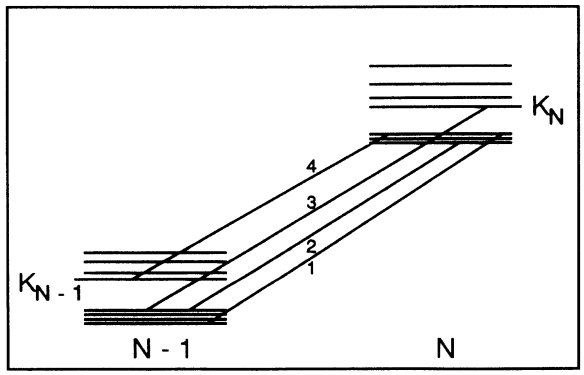

FIG. 7. Energy diagram for the states of $(N-1)$ and N electrons in a situation when states below the gap are equally occupied. The transitions "1" and "2" are energetically allowed ($\mu_L \gg E(N,K_N-1)-E(N-1,0)$ and $E(N,0)-E(N-1,K_{N-1}-1)\gg\mu_R$), and the transitions "3" and "4" are forbidden [$E(N,K_N)-E(N-1,K_{N-1}-1)\gg\mu_L$ and $\mu_R\gg E(N,K_N-1)-E(N-1,K_{N-1})$].

The experimental systems are expected to have between 50 and 100 electrons in the dot, reducing the temperature scale below which the many-body effects are clearly observable from some 100 mK (for eight electrons) to about 30 mK. The gap for center-of-mass excitations is 3.3 K, so their exclusion is well justified at the temperatures in question. Furthermore, the center-of-mass gap is independent of the number of particles whereas gaps for relative excitations decrease as $N^{-1/2}$, making the exclusion of the center of mass even better justified in larger systems.

V. FINITE BIAS EFFECTS

Until now we have concentrated on the transport of electrons through the dot in the linear-response regime, that is, in the limit of zero bias voltage. We have seen how the many-body coherence effects change the width and height of conductance peaks, and how conductance varies as a function of temperature. Now we extend the numerical study to finite bias voltages. Finite bias effects have been studied before in the integer quantum Hall regime.[31]

Current measurements at a finite bias voltage $eV_{sd}=\mu_L-\mu_R$ can yield a great deal of information of the excitation spectrum of the quantum dot. At finite bias voltage we clearly cannot use Eq. (10), which was derived in linear response. Instead, we assume that the transport is described by kinetic equations, which is justified provided that there is no phase coherence between the dot and the leads[32] ($kT\gg\Gamma^L,\Gamma^R$), and provided that inelastic scattering in the dot is negligible. We first solve for the steady-state occupations $n_{N,\alpha}$ and $n_{N-1,\alpha'}$ of quantum levels, and then determine the current. The steady-state equations are

$$\sum_a \Gamma_{a,a'}\{[f_{\rm FD}(E_{N,a}-E_{N-1,a'}-\mu_L)+f_{\rm FD}(E_{N,a}-E_{N-1,a'}-\mu_R)]\times\tfrac{1}{2}[n_{N,a}+n_{N-1,a'}]-n_{N,a}\}=0\ , \quad (23)$$

$$\sum_{a'} \Gamma_{a,a'}\{[f_{\rm FD}(E_{n,a}-E_{N-1,a'}-\mu_L)+f_{\rm FD}(E_{N,a}-E_{N-1,a'}-\mu_R)]\times\tfrac{1}{2}[n_{N,a}+n_{N-1,a'}]-n_{N,a}\}=0\ , \quad (24)$$

where a and a' label the N- and $(N-1)$-electron states, respectively. These equations are scale invariant, and they can be solved by matrix inversion after fixing $n_{N-1,0}$, rather than by finding the eigenvector with zero eigenvalue. The current in the steady state is given by

$$I=\tfrac{1}{4}\sum_{a,a'}\Gamma_{a,a'}[f_{\rm FD}(E_{N,a}-E_{N-1,a'}-\mu_L)-f_{\rm FD}(E_{N,a}-E_{N-1,a'}-\mu_R)]\times[n_{N,a}+n_{N-1,a'}]\ . \quad (25)$$

In some cases it is possible to solve the steady-state equations analytically. The solution is particularly simple if only a few channels are active (Fig. 7). An $(N-1)$-

electron state of the dot is energetically allowed to scatter into a state of N electrons if it can absorb an electron with the appropriate energy from the leads, and vice versa, an N-electron state is energetically allowed to scatter into a state of $(N-1)$ electrons if it can emit an electron with the appropriate energy to the leads. If the ground state of the $(N-1)$-electron system is energetically allowed to scatter into state $|N,K_N-1\rangle$ but not into $|N,K_N\rangle$, and if the ground state of the N-electron system is energetically allowed to scatter into state $|N-1,K_{N-1}-1\rangle$ but not into $|N-1,K_{N-1}\rangle$, then all levels $|N,a=0,\ldots,K_N-1\rangle$ and $|N-1,a'=0,\ldots,K_{N-1}-1\rangle$ are occupied with equal probability $1/(K_N+K_{N-1})$, as can be verified by a direct substitution into Eqs. (23) and (24). These conditions can be met for a suitable choice of μ_L and μ_R, if $E(N-1,K_{N-1})-E(N-1,K_{N-1}-1)\gg E(N,K_N-1)-E(N,0)$ and $E(N,K_N)-E(N,K_N-1)\gg E(N-1,K_{N-1}-1)-E(N-1,0)$, where "$\gg$" means that the difference is much larger than k_BT. In other words, there must be a gap in both the N- and $(N-1)$-electron systems, so that for a suitable choice of μ_L and μ_R no transitions across the gap are allowed (see Fig. 7). This case occurs frequently when the ground state of either the N- or $(N-1)$-electron dot is almost degenerate, as is the case for $N=8$ and $B\approx 5.1$ T.

In Fig. 8(a) we show the current as a function of gate voltage for several bias voltages ranging from 3.2 to 80 μV at the temperature of 40 mK and magnetic field $B=5.1$ T. If the bias voltage is less than the energy separation between the channel involving ground states and the first excited channel [i.e., less than the smaller of the excitation energies of the N- and $(N-1)$-electron systems], the line shape is given by the derivative of the Fermi distribution and agrees with the zero-bias result. When the bias voltage is increased, a more complicated line shape is expected.[31,33] In particular, in Fig. 8(a) at low gate voltages only the well-coupled ground-state channel is active, and when then gate voltage is increased by approximately $(E_{8,3,3}-E_{8,2,3})/e=11$ μV, the excited channel opens for conduction. The opening of the excited channel reduces the probabilities $n_{7,0}$ and $n_{8,0}$ from $\frac{1}{2}$ to $\frac{1}{3}$, and the current actually *decreases* from a relative value of $(\frac{1}{2}+\frac{1}{2})\times 1=1$ to $(\frac{1}{3}+\frac{1}{3})\times 1+(\frac{1}{3}+\frac{1}{3})\times\frac{1}{7}\approx 0.76$. Due to this *"blocking effect,"* measurements at finite bias voltages can be used to detect very weakly coupled channels, which may be difficult to observe by other means. Note that in Fig. 8(a) negative differential resistance is observed over a range of bias voltages when the gate voltage is kept fixed and the bias voltage is varied (e.g., for $V_G=6.08$ V and V_{sd} varying from 50 to 80 μV).

At very low temperatures (but for k_BT still larger than couplings Γ^L and Γ^R) the current peak consists of several plateaus, with the transitions between plateaus indicating the openings and closings of conductance channels [Fig. 8(b)]. Complicated spectra of excited states can be constructed for systems of $(N-1)$, N, and $(N+1)$ electrons by studying the line shapes for the transitions $(N-1)\leftrightarrow N$ and $N\leftrightarrow(N+1)$. Provided that the criteria for the equal occupation of states are met, the relative couplings of different channels can also be easily deduced from the line shapes. However, if the eigenstates are not occupied with equal probability in the steady state, determining the couplings becomes significantly more difficult.

VI. CONCLUSION

In conclusion, we have studied conduction through a weakly coupled dot, $\Gamma^L,\Gamma^R\ll\Delta$, in magnetic fields that are strong enough so that only the lowest Landau level is occupied. Here Γ^L or Γ^R is the effective coupling to the left or right lead, and Δ is the excitation gap. We have studied the problem both numerically and analytically.

In the numerical study we diagonalized exactly the Hamiltonian describing up to eight interacting electrons in a parabolic dot in a strong magnetic field. Identifying the exact eigenstates with particle-hole symmetric counterparts of Laughlin states allows us to extrapolate our results to larger, experimentally relevant systems. The numerical solution allowed us to study the conduction through the dot in two temperature ranges both in linear

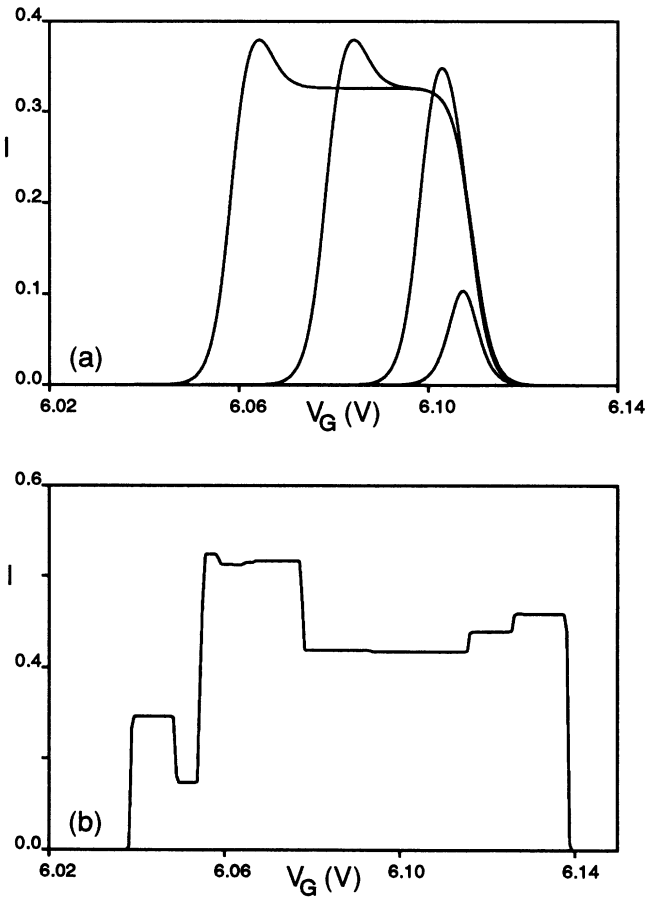

FIG. 8. (a) Current at a finite bias voltage as a function of the gate voltage at $B=5.1$ T and $T=40$ mK ($\hbar\omega_0=1.6$ meV) at bias voltages $\mu_L-\mu_R=3.2$, 16, 50, and 80 μeV. (b) Current at a finite bias voltage as a function of the gate voltage at $B=5.2$ T, $T=0.8$ mK, and $\mu_L-\mu_R=160\mu$eV. Current is expressed in units of $e\gamma/\hbar$. The steps correspond to openings and closings of conductance channels.

response and at a finite bias voltage. We found that in the temperature range $\Gamma^L, \Gamma^R \ll kT \ll \Delta$ the linear-response conductance through the dot is suppressed by many-body coherence effects well below the integer regime values. At higher temperatures, we showed how strongly coupled excited states can lead to anomalous temperature dependence of the conductance, so that the height of a conductance peak may actually *increase* with temperature in contrast to the normal $1/T$ behavior. In the integer case anomalous temperature behavior requires different single-particle couplings,[8] whereas in the fractional case it is a consequence of many-body coherence. At a finite bias voltage we demonstrated how the shapes of current peaks can be used to determine the level spectra and effective many-particle couplings of the quantum dot. Specifically, we showed how transport through a weakly coupled excited state may actually *decrease* the conductance below the low bias value, leading to a negative differential resistance.

In the analytic study we concentrated on linear-response conductance in the intermediate temperature range ($\Gamma^L, \Gamma^R \ll kT \ll \Delta$). Based on the edge-wave theory of excitations in the fractional quantum Hall regime, we predicted that the heights of conductance peaks at simple filling factors $\nu = 1/q$ decrease as $N^{-(q-1)/2}$. This prediction agrees with the numerical results for $\nu = \frac{1}{3}$. At more complicated filling factors we expect to see peaks due to several processes with different suppressions. In particular, at filling factor $\nu = \frac{2}{3}$ we expect that the height of every second peak is independent of N, whereas the other peaks are expected to decay as N^{-3}. In the lowest temperature range, $kT \ll \Gamma^L, \Gamma^R$, the coherence effects do not change the peak heights, but we expect the widths of the Lorentzian peaks of decay as $\Gamma^L + \Gamma^R$, i.e., with the same exponent as the heights of the conductance peaks in the higher temperature range.

ACKNOWLEDGMENTS

We acknowledge helpful discussions with Marc Kastner, Paul McEuen, and Ethan Foxman. The numerical work was performed using the IBM 3090 computer system at the Cornell National Supercomputing Facility at Cornell University, and to a lesser extent on the Cray Y-MP at the National Center for Supercomputing Applications at the University of Illinois in Urbana-Champaign. This work was supported by the National Science Foundation under Grant No. DMR-8913624. One of us (J.K.) also acknowledges the support of the Academy of Finland, and one of us (Y.M.) acknowledges the partial support of the Weizmann Foundation.

*Present address: Physics Department, University of California, Santa Barbara, CA 93106.

†Present address: NEC Research Institute, 4 Independence Way, Princeton, NJ 08540.

[1]U. Meirav, Ph.D. thesis, Massachusetts Institute of Technology, (1990); U. Meirav, M. A. Kastner, and S. J. Wind, Phys. Rev. Lett. **65**, 771 (1990).

[2]P. L. McEuen *et al.*, Phys. Rev. Lett. **66**, 1926 (1991).

[3]P. L. McEuen, E. B. Foxman, J. M. Kinaret, V. Meirau, M. A. Kastner, N. S. Wingreen, and S. J. Wind, Phys. Rev. B **45**, 11 419 (1992).

[4]D. B. Chklovskii, B. I. Shklovskii, and L. I. Glazman, Phys. Rev. B **46**, 4026 (1992).

[5]For a review see H. van Houten, C. W. J. Beenakker, and A. A. M. Staring, in *Single Charge Tunneling,* edited by H. Grabert and M. H. Devoret (Plenum, New York, 1991).

[6]For a review see T. Chakraborty and P. Pietiläinen, *The Fractional Quantum Hall Effect* (Springer, Berlin, 1988).

[7]J. M. Kinaret *et al.*, Phys. Rev. B **45**, 9484 (1992).

[8]Yigal Meir, Ned S. Wingreen, and Patrick A. Lee, Phys. Rev. Lett. **66**, 3048 (1991).

[9]C. W. J. Beenakker, Phys. Rev. B **44**, 1646 (1991).

[10]E. Foxman (private communication).

[11]L. P. Kouwenhoven (private communication).

[12]A. Kumar, S. E. Laux, and F. Stern, Phys. Rev. B **42**, 5166 (1989).

[13]E. H. Rezayi, and A. H. MacDonald, Phys. Rev. B **44**, 8395 (1991).

[14]Ch. Sikorski and U. Merkt, Phys. Rev. Lett. **62**, 2164 (1989).

[15]P. A. Maksym and T. Chakraborty, Phys. Rev. Lett. **65**, 108 (1991).

[16]M. Marcus, *Introduction to Modern Algebra* (Dekker, New York, 1978).

[17]S. A. Trugman and S. Kivelson, Phys. Rev. B **31**, 5280 (1985).

[18]R. B. Laughlin, in *The Quantum Hall Effect,* edited by R. E. Prange and S. M. Girvin (Springer, New York, 1987).

[19]E. H. Rezayi and F. D. M. Haldane (unpublished).

[20]M. D. Johnson and A. H. MacDonald, Phys. Rev. Lett. **67**, 2060 (1991).

[21]S. M. Girvin, Phys. Rev. B **29**, 6012 (1984).

[22]Y. Meir and N. S. Wingreen, Phys. Rev. Lett. **68**, 2512 (1992).

[23]B. Su, V. J. Goldman, and J. E. Cunningham, Science **255**, 313 (1992).

[24]S. Tarucha and Y. Hirayama, Phys. Rev. B **43**, 9373 (1991).

[25]C. W. J. Beenakker, Phys. Rev. Lett. **64**, 216 (1990).

[26]X.-G. Wen, Phys. Rev. B **41**, 12 838 (1991).

[27]X.-G. Wen, Int. J. Mod. Phys. B (to be published).

[28]D. C. Mattis and E. H. Lieb, J. Math. Phys. **6**, 304 (1965).

[29]A. Luther and I. Preschel, Phys. Rev. B **9**, 2911 (1974).

[30]G. Mahan, *Many-Particle Physics,* 2nd ed. (Plenum, New York, 1990).

[31]E. Foxman, Bull. Am. Phys. Soc. **37**, 188 (1992).

[32]D. V. Averin and A. N. Korotkov, Zh. Eksp. Teor. Fiz. **97**, 927 (1990) [Sov. Phys. JETP **70**, 937 (1990)].

[33]N. S. Wingreen, Bull. Am. Phys. Soc. **37**, 134 (1992).

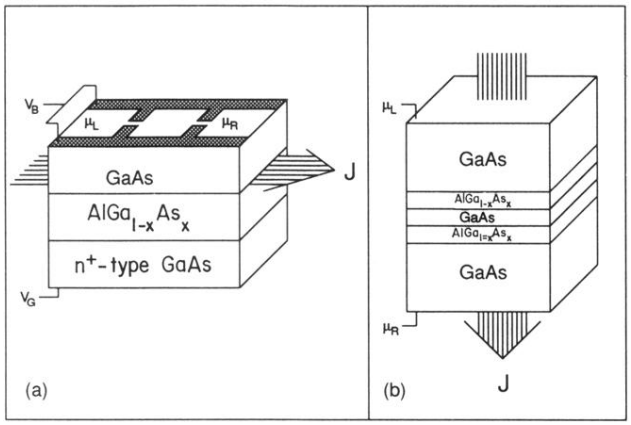

FIG. 1. (a) Planar experimental geometry (Refs. 2 and 11). Negative voltage $-V_T$ is applied to the top gate, which expels electrons in the two-dimensional electron gas and creates a laterally confined quantum dot. The dot is weakly coupled to the leads through electrostatic tunnel barriers, which are also formed using the top gate (i.e., the leads L or R are in the same plane as the dot). The back gate voltage V_G is used to control the number of electrons in the dot. The chemical potentials μ_L and μ_R are set by external reservoirs. (b) Vertical experimental geometry (Refs. 24 and 23). Electrons in the central GaAs layer are weakly coupled to the leads through the narrow $AlGa_{1-x}As_x$ barriers (i.e., the leads L or R are directly above and below the quantum dot). Lateral confinement is obtained through ion bombardment or chemical etching. No gate electrode has been built in.